Experimental Study and Characterization on the Thermo-Electro Multiphysics Coupling Failure of GaN HEMTs Under High-Power Microwave Pulse

Xiangdong Li, *Member, IEEE*, Jiahui Yuan, Hongyue Wang, Zongqi Cai, Weiheng Shao, *Graduate Student Member, IEEE*, Yiqiang Chen, *Member, IEEE*, Xuefeng Zheng, Jincheng Zhang, *Member, IEEE*, and Yue Hao, *Senior Member, IEEE*

***Abstract*—The harsh electromagnetic environment poses a threat to the reliability and safe operation of Gallium nitride (GaN) radio frequency and microwave high-electron-mobility transistors (HEMTs). In this work, we experimentally investigate the thermo-electro multiphysics coupling failure of GaN HEMTs under high-power microwave (HPM) pulse stress. A transient thermal response test and surface electric field distribution measurement methods of GaN HEMTs under HPM stress were proposed. This study demonstrates that at low power HPM injection, the peak temperature of 51 °C is located at the gate–drain access region near the gate side. As the HPM injection power approaches the destruction threshold level, an obvious hot spot of 64 °C is found however strangely in the gate–source access region at the gate edge, in the vicinity of the gate bond pad, or in other words, the input end of the microwave signals. The damage spot is exactly sitting on the hot spot, and also overlapping with the electric field concentration observed by the electric field scanning. This means it is the thermo-electro multiphysics coupling but not solely the thermal burnout that causes the device failure under HPM pulse stress. These findings are of great significance for predicting damage location and improving the reliability design against the complex electromagnetic environments.**

***Index Terms*—Electromagnetic, gallium nitride (GaN), high electron mobility transistor (HEMT), high-power microwave (HPM) injection.**

Manuscript received 17 August 2023; accepted 20 September 2023. Date of publication 6 October 2023; date of current version 24 October 2023. This work was supported in part by the funding of the National Key Research and Development Program of China under Grant 2021YFB3600900, in part by the Youth Fund of the National Natural Science Foundation of China under Grant 62204060, in part by the Key Research and Development Program of Guangzhou under Grant 202103020002, in part by the National Natural Science Foundation of China under Grant 62274043, and in part by the Key Research and Development Program of Guangdong under Grant 2022B0701180002. The review of this article was arranged by Editor M. Meneghini. *(Corresponding authors: Hongyue Wang; Yiqiang Chen.)*

Xiangdong Li, Jiahui Yuan, Xuefeng Zheng, Jincheng Zhang, and Yue Hao are with the Guangzhou Wide Bandgap Semiconductor Innovation Center, Guangzhou Institute of Technology, Xidian University, Guangzhou 510555, China, also with the State Key Laboratory of Wide Bandgap Semiconductor Devices and Integrated Technology, and also with the Key Laboratory of Wide Bandgap Semiconductor Materials and Devices, School of Microelectronics, Xidian University, Xi'an 710071, China.

Hongyue Wang, Zongqi Cai, Weiheng Shao, and Yiqiang Chen are with the Science and Technology on Reliability Physics and Application of Electronic Component Laboratory, The No.5 Electronics Research Institute of the Ministry of Industry and Information Technology Guangzhou, Guandong 510610, China (e-mail: wanghongyue@pku.edu.cn; yiqiang-chen@hotmail.com).

Color versions of one or more figures in this article are available at https://doi.org/10.1109/TED.2023.3319277.

Digital Object Identifier 10.1109/TED.2023.3319277

I. Introduction

GALLIUM nitride (GaN) high-electron-mobility transistors (HEMTs) have been widely adopted in RF and microwave applications like power amplifiers, low noise amplifiers (LNA), and microwave transmitters, thanks to their extraordinary properties including high efficiency, high power output, and low loss. With the rapid development of wireless communication, radar, and pulse power electronic techniques, the electromagnetic environment for HEMTs become more and more harsh, which can even trigger fatal failures [1], [2], [3], [4], [5], [6]. For example, high-power microwave (HPM) pulses can be coupled to the RF front-end via antenna or cable. This results in a very high-power capacity that exceeds the rated power level of the GaN amplifiers. Specifically, this case induces heat accumulation and can even trigger thermoelectric breakdown in AlGaN/GaN HEMTs [7], [8], [9], [10], [11]. Furthermore, in electromagnetic irradiation and electromagnetic interference (EMI) environments, the interference-induced mechanical stress can cause bending and shearing, ultimately resulting in device failure [12], [13].

There are already some works of literature about HPM damage effects on RF and microwave devices. In 1981, James et al. [14] studied the damage effects of GaAs Metal-Semiconductor Field Effect Transistor (MESFETs) under X-band RF spike pulses and concluded that the gate–source short circuit accounts for 60% of the failures. Zhou et al. [8] investigated the relation between the power-to-failure of GaN HEMTs and the HPM pulse duration t_{HPM} that varies

0018-9383 © 2023 IEEE. Personal use is permitted, but republication/redistribution requires IEEE permission.
See https://www.ieee.org/publications/rights/index.html for more information.

Authorized licensed use limited to: Nanjing University. Downloaded on January 10,2024 at 08:47:22 UTC from IEEE Xplore. Restrictions apply.

from 100 to 1000 ns. A thermoelectric failure model was derived and the HPM failure was attributed to serious thermo-mechanical stress in the drain field plate. Chen et al. [7] investigated the degradation behavior of GaN HEMTs under 100 μs HPM pulse duration, and the degradation was found to mainly stem from the electron capture by the traps. Xu et al. [15] successfully extracted the transient thermal response including the maximum channel temperature of gallium arsenide (GaAs) FETs and the maximum input power density of the heat source by a hybrid finite element method (FEM), combining the element-by-element FEM (EBE-FEM) with the preconditioned conjugate gradient (PCG) technique. Li et al. [16] established a circuit model that includes an equivalent physical numerical model of active devices and SPICE models of passive devices. This model describes the nonlinear characteristics of the LNA and provides an empirical formula for predicting the pulsewidth and power that cause LNA damage. As can be seen above, the failure mechanism of GaN HEMTs under HPM pulse stress is still unclear, and the electrical and thermal analysis are usually based on simulation [8], [15], [17]. Plus, the monitoring of the transient thermal response process of the GaN HEMTs under HPM pulses is rarely addressed, which is however vital for HPM applications. Besides, the electric field distribution on the device surface, an important role on analyzing the failure mechanism, is seldom reported. Therefore, advanced thermal-electro multiphysics measurements are urgently needed to unveil the root failure mechanism of GaN HEMTs under HPM pulse stress.

In this study, we experimentally investigated the thermal and electric field distributions of GaN HEMTs under HPM stress by an injection method. The HPM injection system and transient thermo-reflectance imaging (TTI) system were utilized for monitoring the transient junction temperature distribution of GaN HEMT under HPM stress. The electric field probe scanning system was adopted to obtain the surface electric field distribution on the GaN HEMTs surface.

II. Device Structure and RF Performance

The commercial device under test (DUT) is a 6-GHz, 10-W RF HEMT CGH40010 from Wolfspeed [18] with L_G of 0.5 μm, L_{GS} of 1 μm, L_{GD} of 3.5 μm, total W_G of 6.25 mm, and 10 fingers. The absolute maximum rating of the drain–source voltage V_{DS} is 120 V, I_{GMAX} is 4 mA, I_{DMAX} is 1.5 A, $V_{GS(th)}$ is -3 V, gate quiescent voltage $V_{GS(Q)}$ is -2.7 V, power output is 10 W, and upper frequency is 6 GHz. Fig. 1(a) displays the Schematic of the DUT. A detailed cross-sectional scanning electron microscope (SEM) image of the DUT is illustrated by Fig. 1(c)–(e). Usually, the experimental methods for HPM effects include irradiation and injection methods. The injection experiments are less affected by the environment and suitable for device and component level effect research [19]. In our work, the HPM power was injected to the gate of the GaN HEMTs, from the linear region up to the destruction threshold level, during which the RF characteristics were measured. Fig. 1(b) depicts the gain, output power, and maximum power added efficiency (PAE) during the HPM injection to the GaN HEMTs. When driven to the 6.9 dB compression point, the device achieved a maximum power output of 43 dBm (20 W) with a maximum PAE of 62%.

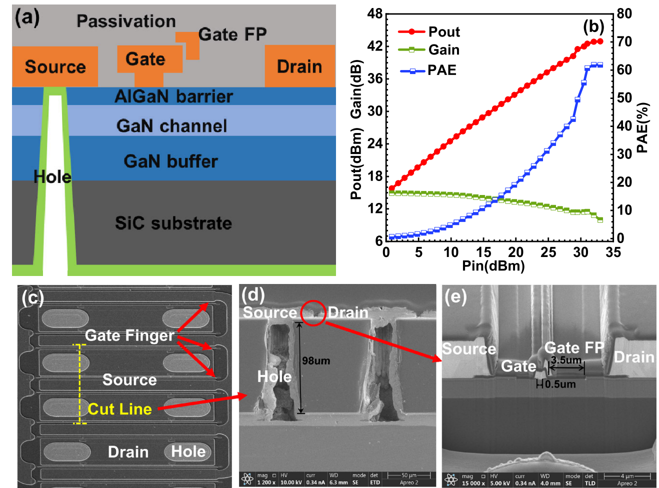

Fig. 1. (a) Schematic cross-sectional view of the GaN HEMTs. (b) RF (radio frequency characteristic) curve of GaN HEMTs during operation. (c) Micrograph. (d) Cross-sectional SEM image along the cutline in (c). (e) Detailed SEM image of the gate area.

III. Transient Thermal Response and Surface Electric Field Distribution Measurement Methods of GaN HEMTs Under HPM Pulse Stress

A. Transient Thermal Response Measurement Methods of GaN HEMTs Under HPM Pulse Stress

The infrared thermal imager technique is commonly used for temperature measurements. However, the maximum spatial resolution of this technique is normally over 3 μm, which is not sufficient for GaN RF HEMTs whose gate length is usually below 1 μm [20]. Besides, the maximum temperature in the GaN HEMTs should be located in the 2DEG channel, because the heat is generated by hot electrons collision on the lattice. In order to obtain the accurate transient temperature distribution of GaN HEMTs under HPM stress, an advanced temperature measurement technique named TTI was used in this work, bearing a high spatial resolution of 400 nm and a high temporal resolution of 100 ns. By this, the temperature in the 2DEG channel can be precisely captured with a 365 nm LED light source [21], [22], [23].

The transient thermal response of the GaN HEMTs under HPM stress was tested using a setup consisting of an HPM injection system and a TTI system. The schematic of this setup is shown in Fig. 2(a).

The HPM injection system was made up of a signal generator, a microwave signal source, a solid-state power amplifier, a circulator, a 40-dB directional coupler, a 15-dB attenuator, and a three-channel oscilloscope. The TTI system includes a 2048 × 2048 pixels CCD camera, an incoherent dispersed low-power UV LED light source with a center wavelength of 365 nm, a 50× UV lens, a thermocouple, and a temperature-controlled piezoelectric stage. The principle of

Authorized licensed use limited to: Nanjing University. Downloaded on January 10,2024 at 08:47:22 UTC from IEEE Xplore. Restrictions apply.

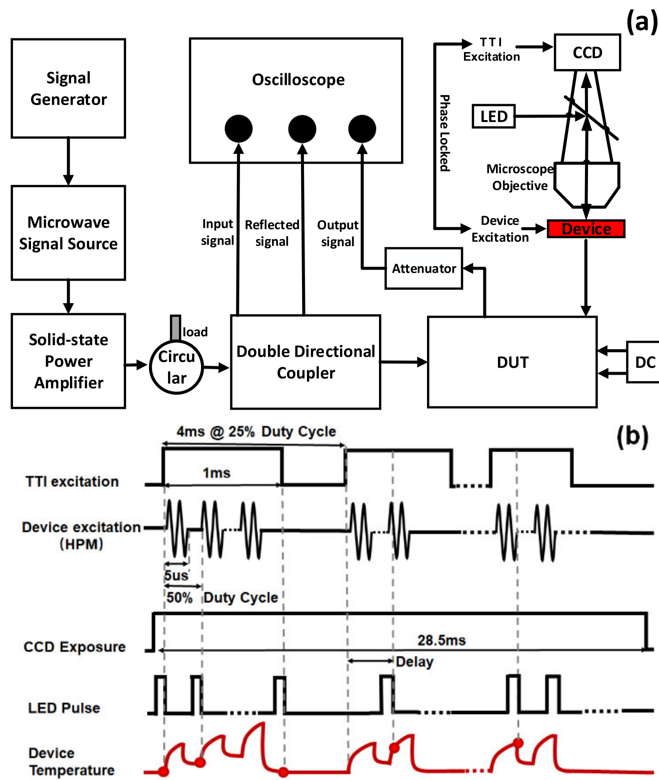

Fig. 2. (a) HPM injection system and TTI (TTI) system. (b) Waveform of various signals under HPM injection and the device temperature transient variation.

thermo-reflectance temperature measurement is based on the change of material reflectivity $\Delta R/R$ with a given temperature rise ΔT, which can be written as follows:

$$\Delta T = \frac{\Delta R}{R \times C_{\text{th}}} \tag{1}$$

where the C_{th} is the thermos-reflectance calibration coefficient.

The testing process is performed in two steps. In the first step, the DUT was placed on the temperature-controlled piezoelectric stage and exposed to UV light from the LED to obtain the initial reflectance value R_0. The C_{th} of the DUT can be derived by the change in the reflected light intensity ΔR with device temperature [24]. The accuracy of this temperature measurement technique is based on how well the C_{th} can be estimated [25]. In this work, the C_{th} of GaN was determined to be $-2.5 \times 10^{-3} \pm 1 \times 10^{-5}$ °C^{-1}, consistent with the report by Pavlidis et al. [21]. In the second step, the signal generator was triggered by TTI to generate a pulse signal, which is used to modulate the solid-state power amplifier to generate a series of HPM pulse signals. The HPM pulses were then injected into the DUT via a circulator and a bi-directional coupler. The temporal signal response was monitored by an oscilloscope. Meanwhile, the TTI system recorded the change in reflected light intensity ΔR of the DUT before and after HPM injection. By using the C_{th} obtained from testing stage I and (1), the transient temperature mapping of the GaN HEMTs under HPM stress can be obtained.

TTI testing is based on lock-in technology to synchronize the excitation signal of the device with the collected signal

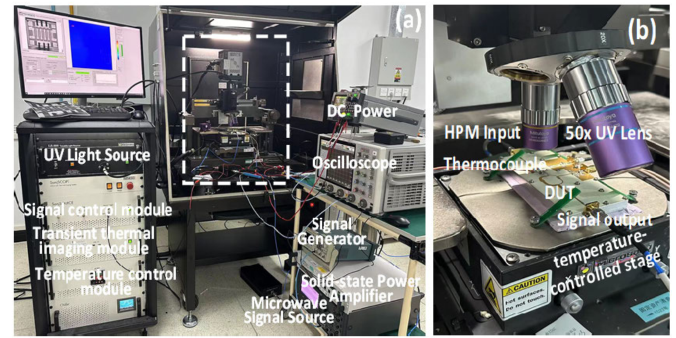

Fig. 3. (a) Photograph of the HPM and TTI system. (b) Details of the dotted box in (a).

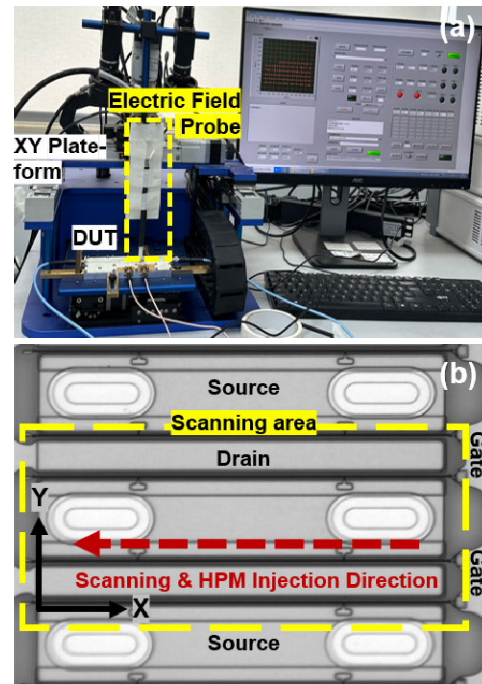

Fig. 4. (a) Image of the setup of the electric field scanning under HPM. (b) HPM signal injection and electric field scanning direction, where the box is the scanning area.

of the detector to obtain a high enough signal-to-noise ratio. Fig. 2(b) illustrates the waveform of these signals under HPM injection and the variation in device temperature. According to current research, the thermal time constant of packaged GaN microwave devices is in the microsecond range [26]. We employed a TTI excitation pulsewidth of 1 ms with a duty cycle of 25%. During the pulsewidth time, the HPM pulse was injected into GaN device with 5 μs pulsewidth and 50% duty cycle. The HPM waveforms are depicted as shown in Fig. 2(b). The frame rate of the transient thermal response system was set to 35 Hz and the CCD exposure time to 28.5 ms. As a result, the system cycles seven times at each CCD exposure time. The temperature distribution of the device within 1 ms is then obtained. During the HPM stress, the quiescent drain bias is 28 V and the gate bias is −2.7 V, and the dc drain current is 200 mA. The photographs of the HPM and TTI systems are shown in Fig. 3.

Authorized licensed use limited to: Nanjing University. Downloaded on January 10,2024 at 08:47:22 UTC from IEEE Xplore. Restrictions apply.

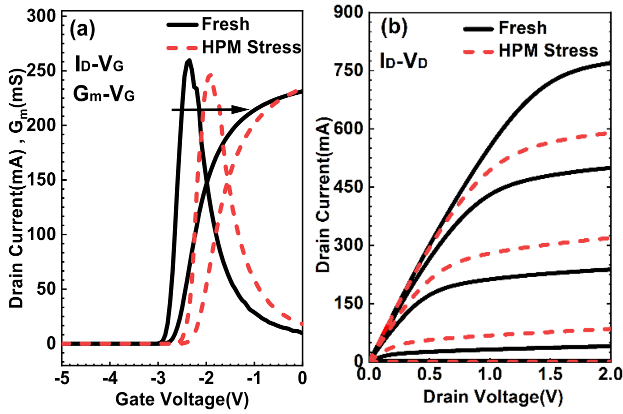

Fig. 5. (a) Transfer and transconductance. (b) Output characteristics of the GaN HEMT before and after the HPM stress.

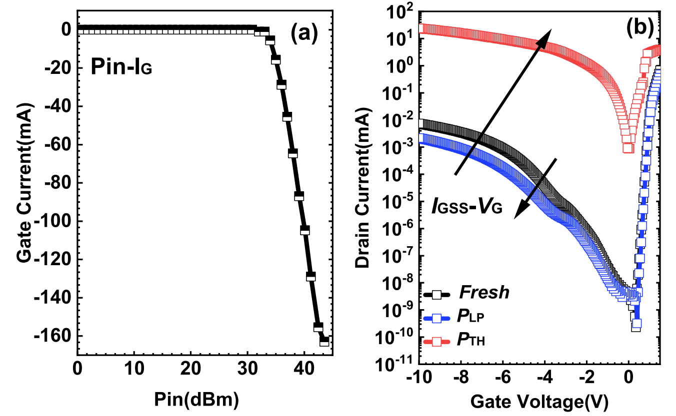

Fig. 6. (a) Gate current versus P_{in} during the HPM injection experiment. (b) Gate current curves of the device in the fresh state, after P_{LP} HPM stress, and close to the P_{TH} HPM stress.

B. Surface Electric Field Distribution Measurement Methods of GaN HEMTs Under HPM Stress

To further analyze the failure mechanism of GaN HEMT under HPM injection, we utilized LANGER electric field probes to conduct electric field scanning on the surface of the GaN HEMTs under HPM injection. The LANGER probes were fixed on an XY platform, and the DUT was placed directly under the probes [27]. The surface electric field distribution of the GaN HEMT was then scanned by moving the XY platform at micrometer level [28]. The LANGER electric field probes were connected to the spectrum analyzer to display the scanning results. Fig. 4(a) shows the experimental setup. Fig. 4(b) displays the injection direction of the HPM signal and the direction of the electric field scanning.

IV. Experimental Results and Discussion

Next, we will demonstrate the experimental results and analyze the electrical degradation, transient temperature response, and surface electric field distribution of the GaN HEMT under HPM stress.

A. Electrical Degradation

Fig. 5(a) shows the I_D–V_G and I_D–V_D curves of the device before and after the HPM stress. It can be seen that the HPM injection causes a decrease of the device's saturation drain current and a threshold voltage V_{TH} positive shift by 0.4 V.

In order to investigate the damage effects of HPM injection on GaN HEMT, we measured the gate current I_G during the HPM injection. As can be seen in Fig. 6(a), when the injected power P_{inject} is low (P_{LP}) and the GaN HEMT in the linear to saturation region, the I_G is almost zero. As the injected power approaches the destruction threshold level of P_{TH}, the I_G starts to degrade toward −180 mA. Fig. 6(b) displays the gate leakage current I_{GSS} before and after HPM injection. After P_{LP} stress, a positive shift of the V_{TH} was observed as shown in Fig. 5(a), concomitant with a decrease in I_{GSS}. This phenomenon can be attributed to the capture of channel electrons by surface states under the gate, driven by the gate–drain electric fields. The captured electrons pull up the potential barrier under the gate, thus inducing the gate

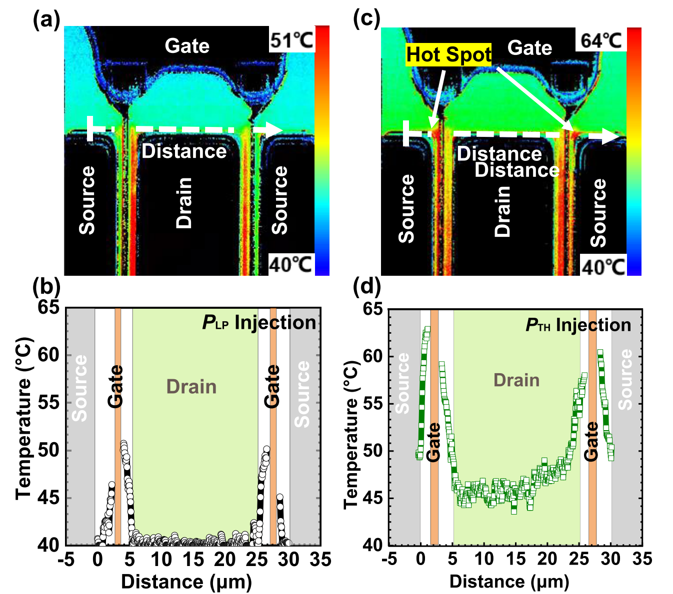

Fig. 7. (a) Temperature distribution of GaN HEMT under P_{LP} stress and (b) its temperature distribution along the horizontal dashed line in (a) from the source to drain and then back to the source. (c) Temperature distribution of the GaN HEMT under P_{TH} stress and (d) its temperature distribution along the horizontal dashed line in (c) from the source to drain and then back to the source.

leakage drop. As the P_{inject} continues to approach the value of P_{TH}, an increase of I_{GSS} by three orders in magnitude was observed, probably stemming from the damage of the Schottky barrier at the gate metal/AlGaN junction.

By changing the pulsewidth and duty cycle of the $P_{injection}$, we obtained the destruction threshold level P_{TH} of the GaN HEMT at different pulsewidth, as shown in the Table I. It can be seen that the P_{TH} decreases with pulsewidth, which is consistent with other HPM injection results [8].

B. Thermal Characteristics

To investigate the failure mechanism of GaN HEMTs under HPM injection, we monitored the thermal distribution during the injection stress. Fig. 7(a) and (c) depicts the temperature distribution of GaN HEMT under P_{LP} and P_{TH} injection, respectively. Fig. 7(b) and (d) displays the

Authorized licensed use limited to: Nanjing University. Downloaded on January 10,2024 at 08:47:22 UTC from IEEE Xplore. Restrictions apply.

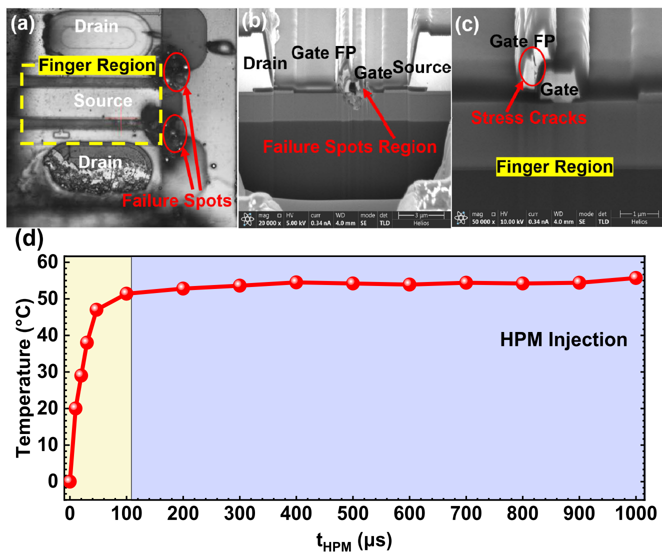

Fig. 8. (a) Micrograph of the GaN HEMT surface after failure under a high-power injection. (b) Cross-sectional SEM image of the gate finger region of the GaN HEMT after failure. (c) Cross-sectional SEM image of the GaN HEMT after burnout. (d) Variation of GaN HEMT channel temperature over time under the 38 W HPM injection.

temperature distribution along the horizontal dashed line from source to drain and then to the source of the HEMTs under the two injection abovementioned, separately. Under P_{LP} injection as shown in Fig. 7(a) and (b), the peak temperature of 51 °C in the GaN channel is located at the gate–drain access region near the gate electrode, which is frequently found in previous reports for GaN HEMTs under stress such as high voltage, self-heating and electrostatic discharge [29], [30]. Under P_{TH} injection as shown in Fig. 7(c) and (d), the increased injection power induces a thermal accumulation near the gate electrode on both the source and drain sides. Furthermore, an obvious hot spot of 64 °C is found in the gate–source access region close to the gate bond pad. This indicates that with the injection power increasing, the peak hot spot in the HEMT shifts from the gate–drain access region to the gate–source access region near the gate pad, which is the microwave signal input port. At this location, high energy loss is caused due to injection power oversaturation.

C. Failure Spots and Analysis

Fig. 8(a) illustrates the surface of the failed GaN HEMT after a high injection power over P_{TH}. The failure spots are located in the vicinity of the gate pad. It should be noted that the failure spots are exactly overlapping with the hot spots found in the transient temperature mappings of Fig. 7(c). Severe damage and even partial melting of the gate electrode is observed by micrograph in Fig. 8(a). The SEM image verifies the failure spot is strangely located in the gate–source access region at the gate edge as shown in Fig. 8(b). Additionally, cracks were observed on the field plate in the finger region, as shown in the SEM image of Fig. 8(c). This phenomenon has also been reported in other studies, which is believed to stem from thermal stress [8].

TABLE I
MEASURED P_{TH} UNDER DIFFERENT HPM PULSEWIDTH

Duty cycle	*Pulse Width* (μs)	P_{TH} (W)
20%	2	89
30%	3	56
50%	5	40
100%	10	25

The transient temperature evolution of the GaN HEMT under HPM injection is shown in Fig. 8(d). The channel temperature rises rapidly within the first 0–100 μs, then gradually saturates after 100 μs. This saturated temperate stays at a relatively low level, which seems impossible to induce the thermal burnout.

Normally, for the HPM pulses with a very short pulsewidth of <10 ns, the GaN HEMT suffers electrical breakdown and has no time to generate heat; for the pulsewidth >10 ns, electro-thermal coupling failure normally occurs; and for the pulsewidth >100 μs, one steady state dominates where thermal equilibrium is established, and some studies state that it stems from hot carrier injection. The pulsewidth used in our experiments is 5 μs with a duty cycle of 50%. Thus, a thermo-electro multiphysics coupling failure instead of thermal burnout is rational to take place in the device.

D. Electric Field Scanning

To verify the hypothesis proposed above, the surface electric field distribution of GaN HEMT under HPM stress is measured. Fig. 9(a) exhibits the electric field distribution on the surface of GaN HEMT in the box area as depicted in Fig. 4(b), under P_{LP} injection. Fig. 9(b) reveals the distribution of the electric field. It can be observed that the electric field at the input end is lower than that at the output end, owing to the amplification of the input signal at the output end.

Fig. 9(c) presents the electric field distribution on the surface of GaN HEMT under P_{TH} injection in the same area, and Fig. 9(d) exhibits the electric field distribution. It can be seen that under P_{TH} injection, the overall surface electric field strength of GaN HEMT is higher than that under P_{LP} injection. It should be noted that the electric field at the signal injection end, i.e., the gate bond pad, is higher than that at the output end in the vicinity of the drain bond pad. This is because, under high-power injection, the injected signals cannot be amplified due to saturation, and most power is reflected back to the input end. A standing wave, located at the corner of the gate bond pad and gate fingers, is thus probably generated due to the large impedance mismatch, leading to a high electric field and failure on the GaN device. This failure mechanism has previously been observed in transmission lines [31]. In view of the relatively low temperature of the hot spot, it is reasonable to confirm that thermal burnout itself, an explanation often used before, cannot easily trigger device failure. Thermo-electro multiphysics coupling failure

Authorized licensed use limited to: Nanjing University. Downloaded on January 10,2024 at 08:47:22 UTC from IEEE Xplore. Restrictions apply.

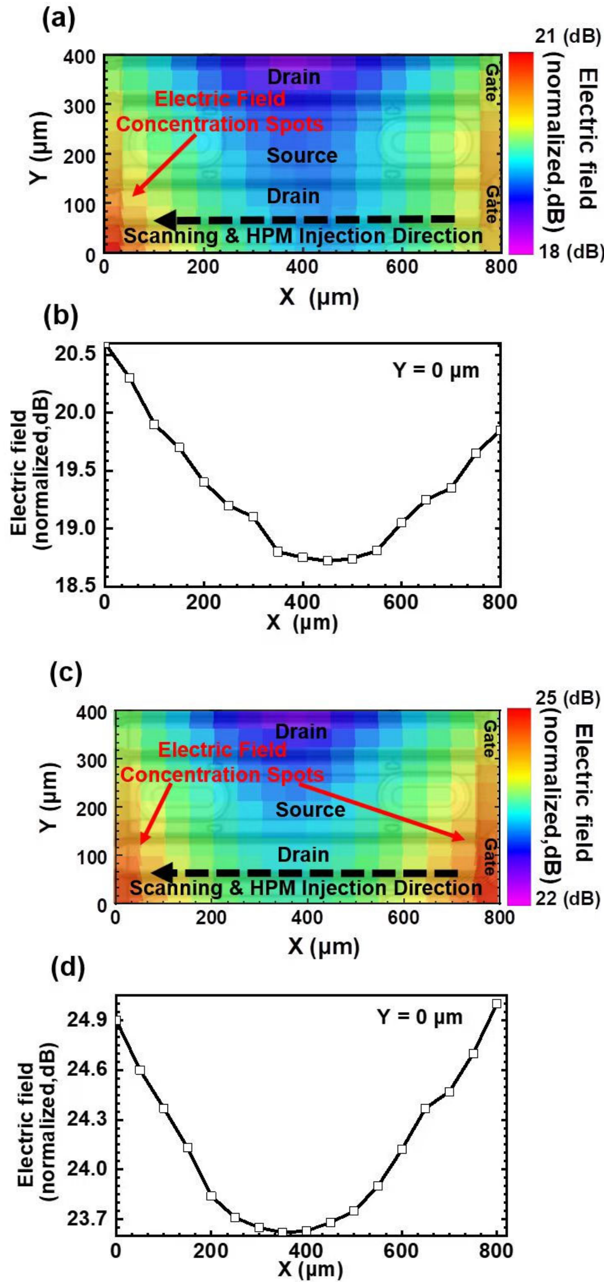

Fig. 9. (a) GaN HEMT surface electric field distribution under P_{LP} HPM stress and (b) its electric field distribution. (c) GaN HEMT surface electric field distribution under P_{TH} HPM stress and (d) its electric field distribution.

of GaN HEMTs under HPM injection is probably the cause of the device failure, as verified by the surface electric filed distribution. GaN material, bearing a strong piezoelectric effect, often suffers a severe inverse piezoelectric effect, which is an electric field driven mechanism where the electric field produces mechanical stress [32], [33]. More extreme failure by electrochemical reaction due to the moisture can also take place [34]. This finding on GaN HEMTs under HPM pulse stress unveils a new failure mechanism and provides an idea to improve the reliability of the devices in the harsh electromagnetic environments.

V. Conclusion

The failure mechanism of the GaN HEMTs under HPM injection on the gate terminal has been investigated in this work by advanced characterization methods including transient thermal imaging test and surface electric field measurement. It has been found that the location of the hot spot changes with injection power. At low power HPM injection, the hot spot of 51 °C was located at the gate–drain access region near the gate side; whereas at high-power HPM injection, a hot spot of 64 °C was found in the gate–source access region at the gate edge, close to the gate bond pad. Since these peak temperatures themselves are insufficient to trigger thermal burnout, a thermo-electro multiphysics coupling failure mechanism of GaN HEMT under high-power microwave HPM stress was proposed, as verified by the electric field concentration at the failure spot detected by the electric field scanning. This inspiring new finding holds significant meanings for localizing failure spots and protecting GaN HEMTs in complex electromagnetic environments in the future.

References

[1] R. Huan, C. Liao, L. Zhou, and J. Luo, "Analysis of electromagnetic leakage of HPM source based on TWPE," in *Proc. IEEE Int. Conf. Comput. Electromagn. (ICCEM)*, Chengdu, China, Mar. 2018, pp. 1–3, doi: 10.1109/COMPEM.2018.8496531.

[2] W. A. Radasky and R. Hoad, "Recent developments in high power EM (HPEM) standards with emphasis on high altitude electromagnetic pulse (HEMP) and intentional electromagnetic interference (IEMI)," *IEEE Lett. Electromagn. Compat. Pract. Appl.*, vol. 2, no. 3, pp. 62–66, Sep. 2020, doi: 10.1109/LEMCPA.2020.3009236.

[3] Y.-Q. Liu, C.-C. Chai, H. Wu, Y.-H. Zhang, C.-L. Shi, and Y.-T. Yang, "Mechanism of AlGaAs/InGaAs pHEMT nonlinear response under high-power microwave radiation," *IEEE J. Electron Devices Soc.*, vol. 8, pp. 731–737, 2020, doi: 10.1109/JEDS.2020.3008816.

[4] P. H. Aaen et al., "Multiphysics modeling of RF and microwave high-power transistors," *IEEE Trans. Microw. Theory Techn.*, vol. 60, no. 12, pp. 4013–4023, Dec. 2012, doi: 10.1109/TMTT.2012.2224366.

[5] W. A. Radasky, C. E. Baum, and M. W. Wik, "Introduction to the special issue on high-power electromagnetics (HPEM) and intentional electromagnetic interference (IEMI)," *IEEE Trans. Electromagn. Compat.*, vol. 46, no. 3, pp. 314–321, Aug. 2004, doi: 10.1109/TEMC.2004.831899.

[6] J. Zhang et al., "Recent advance in long-pulse HPM sources with repetitive operation in S-, C-, and X-bands," *IEEE Trans. Plasma Sci.*, vol. 39, no. 6, pp. 1438–1445, Jun. 2011, doi: 10.1109/TPS.2011.2129536.

[7] Q. Chen et al., "Degradation behavior and trap analysis based on low-frequency noise of AlGaN/GaN HEMTs subjected to radio frequency overdrive stress," *IEEE Trans. Electron Devices*, vol. 68, no. 1, pp. 66–71, Jan. 2021, doi: 10.1109/TED.2020.3040698.

[8] L. Zhou et al., "Investigation on failure mechanisms of GaN HEMT caused by high-power microwave (HPM) pulses," *IEEE Trans. Electromagn. Compat.*, vol. 59, no. 3, pp. 902–909, Jun. 2017, doi: 10.1109/TEMC.2016.2628046.

[9] L. Zhou, Z.-W. San, L. Lin, and W.-Y. Yin, "Electro-thermal-stress interaction of GaN HEMT breakdown induced by high power microwave pulses," in *Proc. Asia–Pacific Int. Symp. Electromagn. Compat. (APEMC)*, vol. 1. Shenzhen, China, May 2016, pp. 642–644, doi: 10.1109/APEMC.2016.7522823.

[10] M. G. Ancona, S. C. Binari, and D. J. Meyer, "Fully coupled thermoelectromechanical analysis of GaN high electron mobility transistor degradation," *J. Appl. Phys.*, vol. 111, no. 7, Apr. 2012, Art. no. 074504, doi: 10.1063/1.3698492.

[11] L. Zhou, S. Zhang, W.-Y. Yin, and J.-F. Mao, "Investigating a thermal breakdown model and experiments on a silicon-based low-noise amplifier under high-power microwave pulses," *IEEE Trans. Electromagn. Compat.*, vol. 58, no. 2, pp. 487–493, Apr. 2016, doi: 10.1109/TEMC.2016.2514441.

Authorized licensed use limited to: Nanjing University. Downloaded on January 10,2024 at 08:47:22 UTC from IEEE Xplore. Restrictions apply.

[12] B. D. Oakes, L. Mattsson, P. Näsman, and A. A. Glazunov, "A systems-based risk assessment framework for intentional electromagnetic interference (IEMI) on critical infrastructures," *Risk Anal.*, vol. 38, no. 6, pp. 1279–1305, Jun. 2018, doi: 10.1111/risa.12945.

[13] W.-F. Zhou, L. Zhou, J.-F. Mao, H.-L. Peng, and W.-Y. Yin, "Analysis of electro-thermal-stress failure of the LDMOS FET under HPM pulses," in *Proc. IEEE Electr. Design Adv. Packag. Syst. Symp. (EDAPS)*, Nara, Japan, Dec. 2013, pp. 205–208, doi: 10.1109/EDAPS.2013.6724425.

[14] S. James, "A study of high power pulsed characteristics of low-noise GaAs MESFET's," *IEEE Trans. Microw. Theory Techn.*, vol. MTT-29, no. 12, pp. 1298–1310, Dec. 1981.

[15] J. Xu, W.-Y. Yin, and J. Mao, "Transient thermal analysis of GaN heterojunction transistors (HFETs) for high-power applications," *IEEE Microw. Wireless Compon. Lett.*, vol. 17, no. 1, pp. 55–57, Jan. 2007, doi: 10.1109/LMWC.2006.887261.

[16] L. Fuxing et al., "Study on high power microwave nonlinear effects and degradation characteristics of C-band low noise amplifier," *Microelectron. Rel.*, vol. 128, Jan. 2022, Art. no. 114427, doi: 10.1016/j.microrel.2021.114427.

[17] A. Wang et al., "Impact of intrinsic stress in diamond capping layers on the electrical behavior of AlGaN/GaN HEMTs," *IEEE Trans. Electron Devices*, vol. 60, no. 10, pp. 3149–3156, Oct. 2013, doi: 10.1109/TED.2013.2275031.

[18] (2020). *Wolfspeed, CGH40010, Datasheet*. [Online]. Available: https://www.wolfspeed.com/cgh40010/

[19] D. Nitsch, M. Camp, F. Sabath, J.-L. T. Haseborg, and H. Garbe, "Susceptibility of some electronic equipment to HPEM threats," *IEEE Trans. Electromagn. Compat.*, vol. 46, no. 3, pp. 380–389, Aug. 2004, doi: 10.1109/TEMC.2004.831842.

[20] S. A. Merryman and R. M. Nelms, "Diagnostic technique for power systems utilizing infrared thermal imaging," *IEEE Trans. Ind. Electron.*, vol. 42, no. 6, pp. 615–628, Dec. 1995, doi: 10.1109/41.475502.

[21] G. Pavlidis, D. Kendig, E. R. Heller, and S. Graham, "Transient thermal characterization of AlGaN/GaN HEMTs under pulsed biasing," *IEEE Trans. Electron Devices*, vol. 65, no. 5, pp. 1753–1758, May 2018, doi: 10.1109/TED.2018.2818621.

[22] B. Chatterjee et al., "Nanoscale electro-thermal interactions in AlGaN/GaN high electron mobility transistors," *J. Appl. Phys.*, vol. 127, no. 4, Jan. 2020, Art. no. 044502, doi: 10.1063/1.5123726.

[23] M. G. Burzo, P. L. Komarov, and P. E. Raad, "Noncontact transient temperature mapping of active electronic devices using the thermoreflectance method," *IEEE Trans. Compon. Packag. Technol.*, vol. 28, no. 4, pp. 637–643, Dec. 2005, doi: 10.1109/TCAPT.2005.859738.

[24] M. J. Tadjer et al., "GaN-on-diamond HEMT technology with T_{AVG} = 176 °C at $P_{DC,max}$ = 56 W/mm measured by transient thermoreflectance imaging," *IEEE Electron Device Lett.*, vol. 40, no. 6, pp. 881–884, Jun. 2019, doi: 10.1109/LED.2019.2909289.

[25] S. Martin-Horcajo, J. W. Pomeroy, B. Lambert, H. Jung, H. Blanck, and M. Kuball, "Transient thermoreflectance for gate temperature assessment in pulse operated GaN-based HEMTs," *IEEE Electron Device Lett.*, vol. 37, no. 9, pp. 1197–1200, Sep. 2016, doi: 10.1109/LED.2016.2595400.

[26] K. R. Bagnall, O. I. Saadat, S. Joglekar, T. Palacios, and E. N. Wang, "Experimental characterization of the thermal time constants of GaN HEMTs via micro-Raman thermometry," *IEEE Trans. Electron Devices*, vol. 64, no. 5, pp. 2121–2128, May 2017, doi: 10.1109/TED.2017.2679978.

[27] N. N. Mai-Khanh, S. Nakajima, T. Iizuka, Y. Mita, and K. Asada, "Noninvasive localization of IGBT faults by high-sensitivity magnetic probe with RF stimulation," *IEEE Trans. Instrum. Meas.*, vol. 67, no. 4, pp. 745–753, Apr. 2018, doi: 10.1109/TIM.2017.2789038.

[28] W. Shao et al., "An ultrawideband asymmetric calibration method for a simultaneously electromagnetic near-field probing system," *IEEE Trans. Microw. Theory Techn.*, vol. 71, no. 3, pp. 1083–1092, Mar. 2023, doi: 10.1109/TMTT.2022.3214847.

[29] R. Singh, K. Aditya, A. Veloso, B. Parvais, and A. Dixit, "Experimental evaluation of self-heating and analog/RF FOM in GAA-nanowire FETs," *IEEE Trans. Electron Devices*, vol. 66, no. 8, pp. 3279–3285, Aug. 2019, doi: 10.1109/TED.2019.2924439.

[30] S. Choi, E. R. Heller, D. Dorsey, R. Vetury, and S. Graham, "The impact of bias conditions on self-heating in AlGaN/GaN HEMTs," *IEEE Trans. Electron Devices*, vol. 60, no. 1, pp. 159–162, Jan. 2013, doi: 10.1109/TED.2012.2224115.

[31] D. A. de Wolf, "Surface losses in transmission lines," *IEEE Antennas Propag. Mag.*, vol. 34, no. 4, pp. 22–26, Aug. 1992, doi: 10.1109/74.153561.

[32] J. A. del Alamo and J. Joh, "GaN HEMT reliability," *Microelectron. Rel.*, vol. 49, nos. 9–11, pp. 1200–1206, Sep. 2009, doi: 10.1016/j.microrel.2009.07.003.

[33] E. Zanoni, M. Meneghini, A. Chini, D. Marcon, and G. Meneghesso, "AlGaN/GaN-based HEMTs failure physics and reliability: Mechanisms affecting gate edge and Schottky junction," *IEEE Trans. Electron Devices*, vol. 60, no. 10, pp. 3119–3131, Oct. 2013, doi: 10.1109/TED.2013.2271954.

[34] F. Gao, C. V. Thompson, J. A. D. Alamo, and T. Palacios, "Role of electrochemical reactions in the degradation mechanisms of AlGaN/GaN HEMTs," in *Proc. CS MANTECH Int. Conf. Compd. Semicondectors Manuf. Technol.*, 2014, pp. 29–32.

Authorized licensed use limited to: Nanjing University. Downloaded on January 10,2024 at 08:47:22 UTC from IEEE Xplore. Restrictions apply.